Nonidentical protons

T. Mart* and A. Sulaksono
Departemen Fisika, FMIPA, Universitas Indonesia, Depok 16424, Indonesia
(Received 1 August 2012; revised manuscript received 1 February 2013; published 28 February 2013)

We have calculated the proton charge radius by assuming that the real proton radius is not unique and the radii are randomly distributed in a certain range. This is performed by averaging the elastic electron-proton differential cross section over the form factor cutoff. By using a dipole form factor and fitting the middle value of the cutoff to the low-Q^2 Mainz data, we found the lowest χ^2/N for a cutoff $\Lambda = 0.8203 \pm 0.0003$ GeV, which corresponds to a proton charge radius $r_E = 0.8333 \pm 0.0004$ fm. The result is compatible with the recent precision measurement of the Lamb shift in muonic hydrogen as well as recent calculations using more sophisticated techniques. Our result indicates that the relative variation of the form factor cutoff should be around 21.5%. Based on this result we have investigated effects of the nucleon radius variation on the symmetric nuclear matter (SNM) and the neutron star matter (NSM) by considering the excluded volume effect in our calculation. The mass-radius relation of a neutron star is found to be sensitive to this variation. The nucleon effective mass in the SNM and the equation of state of both the SNM and the NSM exhibit a similar sensitivity.

DOI: 10.1103/PhysRevC.87.025807 PACS number(s): 26.60.−c, 21.65.−f, 13.40.Gp, 14.20.Dh

I. INTRODUCTION

The recent precise measurement of the Lamb shift in a muonic hydrogen atom [1] has sparked a controversy, because this measurement yields a smaller proton charge radius, i.e., $r_E = 0.84184(67)$ fm. This radius is significantly smaller than the standard CODATA value [2], $r_E = 0.8768(69)$ fm, which is based on the measurements of the Lamb shift in an electronic (conventional) hydrogen atom, as well as the results from elastic electron-proton scatterings. The latest precise measurement of elastic electron-proton scattering at MAMI, Mainz, which yields $r_E = 0.879(5)_{\text{stat.}}(4)_{\text{syst.}}(2)_{\text{model}}(4)_{\text{group}}$ fm [3], clearly supports the CODATA value. Considerable efforts [4–21] have been devoted to attacking this proton radius problem. References [4,5], for instance, propose that the off-shell form factors of the proton could generate large polarizability contributions to the proton structure and eventually could solve the problem, as the effect would only appear in the case of muonic hydrogen. However, a different opinion has been put forward in Ref. [22], in which the off-shell effect is shown to be not sufficiently large to reduce the discrepancy in the radii found in muonic and conventional hydrogen atoms. It is interesting to note that Ref. [22] also concludes that the resolution of this problem must lie elsewhere, perhaps in re-analyses of the older experiments. Furthermore, QED is believed to be more precise than QCD, and the techniques and methods of the Lamb shift measurement in muonic hydrogen as well as electron-proton scattering are beyond any doubt [23]. Therefore, it is urgent to reinvestigate the prevailing methods of extracting the proton charge radius. This idea was recently proposed by a number of research groups [24,25]. Nevertheless, surprisingly, none of them has questioned the idea of the "radius" itself.

The radius of a proton is defined in accordance with our imagination that the proton has a spherical form. However, recent investigations have revealed that protons could deform from a spherical shape, like nuclei in nuclear physics. This originates from the relativistic motion of the spin-1/2 quarks inside the proton [26], although there is also a claim that a pure s-wave nucleon model, with $l = 0$ and thus perfectly spherical, could be constructed [27]. Meanwhile, in the liquid drop model it is also customary to assume the variation of the proton and neutron radii in order to explain, e.g., the polarized electric dipole moment in the reflection asymmetric nuclei [28]. Obviously, the definition of the radius would be blurred if the proton were not spherical.

On the other hand, the fluctuating size of the proton has become an important idea in explaining oscillating color transparency [29]. The idea behind this fluctuating size is that in the proton-nucleus scattering the high-energy protons that scattered at wide angles should be "small." However, there is also a certain process, in which the protons must be "large" and the amplitude of this process will increase with increasing proton sizes. Using this idea, the oscillating transparency found in the experiment in [30], which is defined as the ratio of the proton-proton scattering cross sections off the nucleus to those off the proton at 90° as a function of energy, can be successfully reproduced [29].

Based on the above background, in this paper we propose a calculation of the proton charge radius by assuming that protons do not have identical radii; they vary in a certain range. To simplify the problem we further assume that the radii are randomly distributed around their average value. Practically, as the proton radius enters the cross section via the charge form factor, we can perform this calculation by taking the form factor cutoff as the corresponding variable. We believe that further corrections could enter the cross-section formulation. However, for the present exploratory study we also believe that our assumption will be sufficient.

We note that our result is in agreement with that obtained from muonic hydrogen [1]. A more careful measurement was carried out at Paul Scherer Institute and the result was just published [32]. It is interesting to note that the latter is still

*terry.mart83@gmail.com

consistent with the previous measurement [1], indicating that the proton radius extracted from muonic hydrogen would hardly change. Therefore, the discrepancy between our result and the electronic hydrogen experiment is still outstanding and more efforts are required to alleviate this problem.

Whereas a 5% difference in the proton radius could trigger a strong controversy in hadronic studies, it is quite ironic to realize that in nuclear and neutron star matter (NSM) investigations protons and neutrons are traditionally considered "point particles." Effects of the nucleon structures are only considered in the so-called *excluded volume effect* (EVE) model [33–39]. In this model the total volume occupied by N nucleons, i.e., Nv_N, is subtracted from the nuclear matter volume V, so that the effective volume available for the nucleon motion is reduced to $V - Nv_N$, where v_N is the volume of a nucleon. Of course, the volume of the nucleon itself decreases as the matter density increases. However, surprisingly, there has been no unique definition of the radius in free space, i.e., at zero density. For instance, Ref. [34] used the proton radii $r_p = 0.80$, 0.70, and 0.60 fm to study the EVE on the equation of state (EOS) of homogeneous hadronic matter, whereas Ref. [33] used $r_p = 0.63$ fm to study the effect on the EOS of nuclear matter. Nevertheless, all studies indicate that the effect is non-negligible. In fact, Ref. [34] found that the effect can enlarge the range of applicability of the quark-meson-coupling (QMC) model. Thus, it would be very interesting to study the EVE by using our knowledge obtained from the elastic electron-proton scattering process.

In Sec. II of this paper we explain the procedure for extracting the proton charge form factor. Section III briefly discuss the possible future experiment for refining the present calculation. In Sec. IV we investigate effects of the nucleon radius variation in the neutron star and symmetric nuclear matter (SNM). We summarize and conclude our findings in Sec. V.

II. EXTRACTION OF THE PROTON RADIUS FROM ELECTRON-PROTON SCATTERING

The differential cross section for elastic electron-proton scattering can be efficiently written in terms of the Sachs electric and magnetic form factors, $G_{E,p}$ and $G_{M,p}$, as [40]

$$\frac{d\sigma}{d\Omega} = \left(\frac{d\sigma}{d\Omega}\right)_{\text{Mott}} \frac{1}{(1+\tau)}\left[G^2_{E,p}(Q^2) + \frac{\tau}{\epsilon}G^2_{M,p}(Q^2)\right], \quad (1)$$

where the Mott cross section,

$$\left(\frac{d\sigma}{d\Omega}\right)_{\text{Mott}} = \frac{E'}{E}\frac{\alpha^2}{4E^2}\frac{\cos^2(\theta/2)}{\sin^4(\theta/2)}, \quad (2)$$

describes the elastic scattering of a point-like particle. The notation $\epsilon = [1 + 2(1+\tau)\tan^2(\theta/2)]^{-1}$ denotes the virtual photon polarization, $Q^2 = 4EE'\sin^2(\theta/2)$ is the square of the virtual photon momentum transfer, $\tau = Q^2/4m_p^2$, m_p is the proton mass, and E (E') represents the electron initial (final) laboratory energy with scattering angle θ.

Because we do not focus on the problems of extracting the magnetic form factor, we use the phenomenological scaling $G_{M,p} = \mu_p G_{E,p}$, where μ_p is the proton anomalous magnetic moment, to simplify Eq. (1) to

$$\frac{d\sigma}{d\Omega} = \left(\frac{d\sigma}{d\Omega}\right)_{\text{Mott}} \frac{1}{(1+\tau)}\left[1 + \frac{\tau}{\epsilon}\mu_p^2\right]G^2_{E,p}(Q^2, \Lambda), \quad (3)$$

assuming identical charge distributions in the protons, i.e., identical electric and magnetic radii, where Λ is the corresponding cutoff.

However, if the the proton sizes were not identical, and if we assume that they were randomly distributed near their middle value, then Eq. (1) must be averaged over all proton sizes, i.e., averaged over the form factor cutoff Λ,

$$\left\langle\frac{d\sigma}{d\Omega}\right\rangle = \left(\frac{d\sigma}{d\Omega}\right)_{\text{Mott}} \frac{1}{(1+\tau)}\left[1 + \frac{\tau}{\epsilon}\mu_p^2\right]\left\langle G^2_{E,p}(Q^2, \Lambda_1)\right\rangle, \quad (4)$$

where

$$\left\langle G^2_{E,p}(Q^2, \Lambda_1)\right\rangle = \frac{1}{2\Delta\Lambda}\int_{\Lambda_1-\Delta\Lambda}^{\Lambda_1+\Delta\Lambda} G^2_{E,p}(Q^2, \Lambda)d\Lambda, \quad (5)$$

and $2\Delta\Lambda$ represents the range of the cutoff variation around the middle value Λ_1.

Experimental measurements for decades have indicated that the square root of this average can be parameterized by means of a dipole form,

$$\left\langle G^2_{E,p}(Q^2, \Lambda_1)\right\rangle^{1/2} \approx \left(1 + \frac{Q^2}{\Lambda_1^2}\right)^{-2}, \quad (6)$$

where $\Lambda_1^2 = 0.71$ GeV^2 is often called the standard dipole form factor, from which one obtains the proton electric radius by calculating the form factor slope at the real photon point,

$$r_E \equiv \left\langle r^2_{E,p}\right\rangle^{1/2} = \left(-6\frac{dG_{E,p}(Q^2)}{dQ^2}\bigg|_{Q^2=0}\right)^{1/2}. \quad (7)$$

At this stage it is important to note that after the operation of modern continuous beam accelerators, such as MAMI in Mainz and CEBAF at the Jefferson Laboratory, significant deviation from the standard dipole form factor has been observed. To account for this deviation a number of new fits and models have been proposed. This includes modifications of the dipole form [43,44], as well as the introduction of more physical ingredients in the form factor [42,45]. There seems to be no need to keep the original dipole form to fit both electric and magnetic form factors, especially for a global fit to all data, as the standard dipole is considered to be just a phenomenological approximation. Furthermore, the choice of the dipole form also seems to be trivial.

However, in the nonrelativistic limit as well as in the Breit frame the dipole form factor is related to an exponentially decaying charge distribution via the Fourier transform. The exponentially decaying behavior is found in most natural phenomena, from radioactive decay rate to atmospheric pressure on Earth. Some phenomena in social science also exhibit this behavior. Thus, we believe that in our present case a dipole form factor looks more natural and a deviation from such a natural phenomenon requires a rigorous physical concept.

Furthermore, it is also important to emphasize here that the determination of the slope at $Q^2 = 0$ given by Eq. (7) requires

very good knowledge of $G_{E,p}(Q^2)$ at very low Q^2. As a consequence, the more closely we can approach the real photon point experimentally, the more reliably we can determine the proton charge radius. Therefore, the latest and most accurate measurement of the elastic electron-proton scattering with low energy and low Q^2 at MAMI [3] provides very suitable experimental data for our present discussion.

We begin with Eq. (6), which implies that the experimentally observed form factor is in fact an average of the genuine form factor, which one actually should use in Eq. (7) in order to get the real proton radius. As a consequence, the proton radius extracted in this way should be considered an averaged radius.

To investigate the effect of averaging the form factor given by Eq. (5), let us use the standard dipole form factor to calculate $\langle G^2_{E,p}(Q^2, \Lambda_1)\rangle$ in Eq. (5). Note that if we use a dipole form, the magnitude of the relative variations of both radius r and cutoff Λ are equal, i.e.,

$$\left|\frac{\Delta\Lambda}{\Lambda}\right| = \left|\frac{\Delta r}{r}\right|, \tag{8}$$

provided that the variations are not extremely large.

The result is shown in Fig. 1, where we compare our calculations obtained with the cutoff variations $\Delta\Lambda$ from 0 up to 40% of its standard value with experimental data. Note that for the sake of simplicity we use the latest result from the Mainz experiment [3], which provides the latest and most accurate data in the low-Q^2 region, and the result of extraction from the world electron-proton scattering data with two-photon exchange effects included [42], which represents the previous measurements. We use the result obtained from the standard Rosenbluth separation technique for the Mainz data, in order to reduce the model dependency of the data. The $G_{E,p}$ data extracted in Ref. [42] are, of course, model dependent. However, in this paper they are only used for the purpose of comparison and are not included in the fitting database as described in the following discussion.

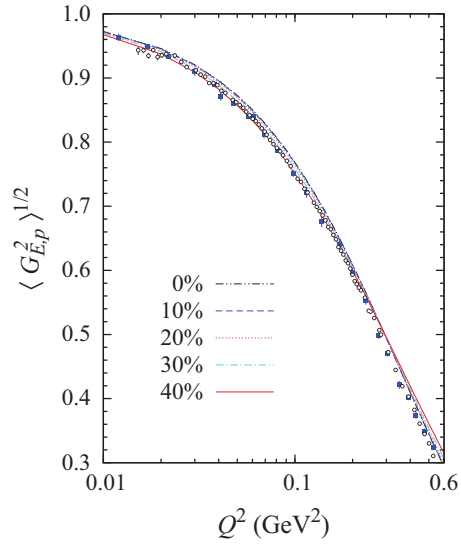

FIG. 1. (Color online) Square root of the averaged $G^2_{E,p}$ calculated from Eq. (5) for different values of the relative variation $\Delta\Lambda/\Lambda_1$ (shown here) compared with experimental data. Experimental data are taken from Refs. [3] (open circles) and [42] (filled squares).

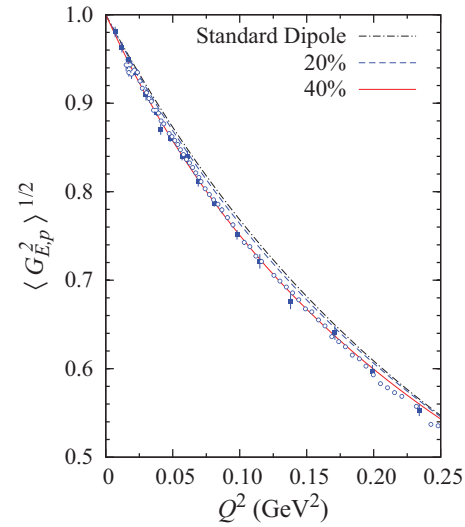

FIG. 2. (Color online) As Fig. 1, but limited to $Q^2 \leqslant 0.25$ GeV^2. The results obtained for two values of $\Delta\Lambda/\Lambda_1$ are compared with the standard dipole form factor and experimental data. Note the linear scale for the Q^2 axis.

It is obvious from Fig. 1 that the result shows a variance to the standard dipole form. For $Q^2 \gtrsim 0.25$ GeV^2 we observe that the averaged form factors are larger than the standard dipole one (i.e., $\Delta\Lambda/\Lambda = 0$); increasing the relative variation will increase the form factor. However, for $Q^2 \lesssim 0.25$ GeV^2 we observe a different behavior, i.e., the form factor decreases as the variation increases. Because the decrease is relatively small, it is almost invisible in Fig. 1. Therefore, in Fig. 2 we increase the resolution of the $\langle G^2_{E,p}(Q^2, \Lambda_1)\rangle^{1/2}$ axis by limiting $Q^2 \lesssim 0.25$ GeV^2, where we can clearly see the effect of variation, i.e., for the relative variation of 40% the agreement with experimental data is almost perfect.

Although the agreement of the solid curve with experimental data in Fig. 2 could be fortuitous, the most important message is that the standard dipole form factor is still valid at low Q^2, provided that the corresponding cutoff must be averaged with relative variation $\Delta\Lambda/\Lambda_1 = 40\%$. We believe that this is crucial because extraction of the proton charge radius is always plagued with many complicated corrections, especially under a high-Q^2 regime, as discussed above. In view of this, in what follows, we only use the MAMI data and limit the Q^2 up to 0.25 GeV^2.

It is apparent from Eq. (5) and Fig. 2 that for each value of $\Delta\Lambda$ we can optimize the form factor cutoff Λ_1 in order to further improve the agreement of our calculation with experimental data. For this purpose we can calculate the standard χ^2/N, which measures the agreement of our calculation with experimental data. The result as a function of the proton radius (translated from Λ_1) and $\Delta\Lambda/\Lambda_1$ is displayed in Fig. 3. It is obvious that χ^2/N has only one minimum, located by the intersection of the two dashed lines.

To locate this minimum accurately we fit the value of Λ_1 using the CERN-MINUIT code and scan the relative variation

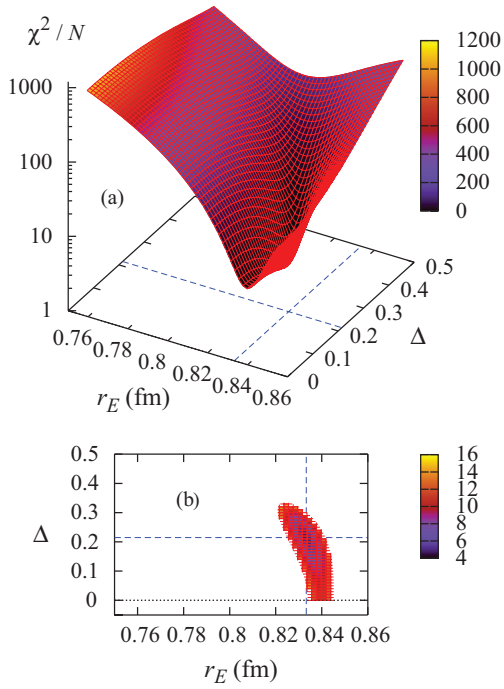

FIG. 3. (Color online) (a) The obtained χ^2/N values as functions of the proton charge radius r and $\Delta \equiv \Delta\Lambda/\Lambda_1$. (b) The projection of χ^2/N on the $r - \Delta$ plane for $\chi^2/N \leqslant 16$. The intersection of the vertical and horizontal dashed lines locates the minimum position of χ^2/N, which is accurately shown in Fig. 4.

$\Delta\Lambda/\Lambda_1$ from 0% to 50%, with a 2.5% step, simultaneously, where the value of Λ_1 is allowed to vary between 0.80 and 0.90. Although this choice seems to be arbitrary, in our fits we found that the Λ_1 value never reaches both upper and lower limits. For $\Delta\Lambda/\Lambda_1 = 0\%$ (50%) the cutoff value is obtained as 0.8142 (0.8493) GeV, which corresponds to the proton charge radius of 0.8396 (0.8048) fm.

Having finished the scanning process we observe that the obtained χ^2/N forms a parabola with the minimum value at $\Delta\Lambda/\Lambda_1 = 21.5\%$ and $\Lambda_1 = 0.8203$ GeV. This corresponds to a relative variation of proton radius $\Delta r_E/r_E \approx 21.5\%$, from Eq. (8), and a proton radius of $r = 0.8333$ fm, from Eq. (7). The complete result of this scanning process is depicted in Fig. 4(a). To increase the accuracy, we have refined the $\Delta\Lambda/\Lambda_1$ step to 0.005, which is equivalent to $\Delta r_E = \pm 0.0003$ fm, in the vicinity of the minimum. Therefore, our calculation would produce the best agreement with experimental data if we used $r_E = 0.8333 \pm 0.0004$ fm, where we have added the error bar coming from the fitting process (Δr obtained from the MINUIT package). The present result is very interesting because it corroborates most of the latest findings that exploit more sophisticated techniques [24,25].

We have also performed the above procedure to find the proton magnetic radius. It is well known that the experimental data in this case are notoriously inaccurate, especially at $Q^2 \approx 0$. As a consequence, we did not use the four lowest Q^2 data points from Ref. [31], because most of them cannot be renormalized to μ_p at the real photon point. For comparison with the charge radius, we display the result in Fig. 4(b).

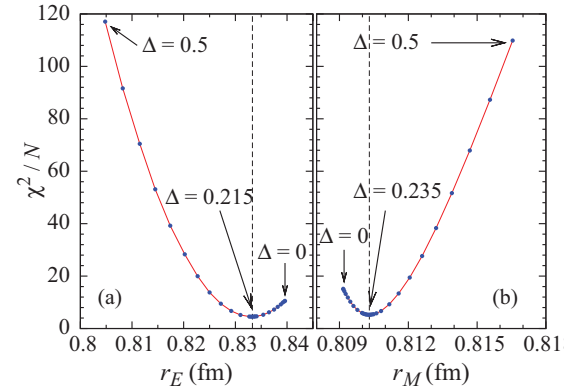

FIG. 4. (Color online) χ^2/N as a function of the obtained proton (a) charge and (b) magnetic radii. The lowest and highest values of relative variation in the form factor cutoff, $\Delta \equiv \Delta\Lambda/\Lambda_1$, are indicated. Vertical lines indicate the minimum positions of χ^2/N. The corresponding Δ values are also shown.

Obviously, the trend is different as in the case of the charge radius. In the case of the charge form factor, increasing the relative variation is required to decrease the magnitude of $G_{E,p}$ in order to reproduce experimental data (see Fig. 2). In contrast to this, the relative variation of the radius is required to increase the magnitude of $G_{M,p}$, in order to reproduce the data.

As shown in Fig. 4 we obtain $r_M = 0.8103 \pm 0.0004$ fm, which is smaller than the result extracted from the dispersion relation, i.e., $0.84^{+0.01}_{-0.02}$ fm [24]. Nevertheless, our magnetic radius is much larger than that obtained from direct extraction of the Mainz data, i.e., 0.777 ± 0.013 fm [3]. However, if the Friedrich-Walcher parametrization [43] was used in the latter, the magnetic radius would increase to 0.807 ± 0.02 fm [31], which is apparently in good agreement with our finding. We believe that the less accurate magnetic form factor extracted from the electron-proton scattering could be the origin of the large variance in the extracted magnetic radii found in the literature.

III. EXPECTED FUTURE ELECTRON-PROTON SCATTERING EXPERIMENTS

Because the mathematical formula of the proton charge form factor is, in principle, not known, determination of the proton radius using Eq. (7) requires very good knowledge of the proton form factor to a very low-Q^2 region. Thus, the real challenge for future experiments is to extend the current experimental data to this kinematics. The situation is exhibited in Fig. 5, where we compare the result for the 21.5% proton radius variation obtained in the previous section and various available parametrizations with experimental data [3,42]. It is obvious from this figure that the Mainz data tend to deviate from our present result, whereas, surprisingly, the data extracted in Ref. [42] show a very good agreement with our calculation. We note that Ref. [42] used polynomial expansion to parametrize the form factor during the extraction. Therefore, we believe that the agreement with the present calculation as exhibited in Fig. 5 could not be a coincidence.

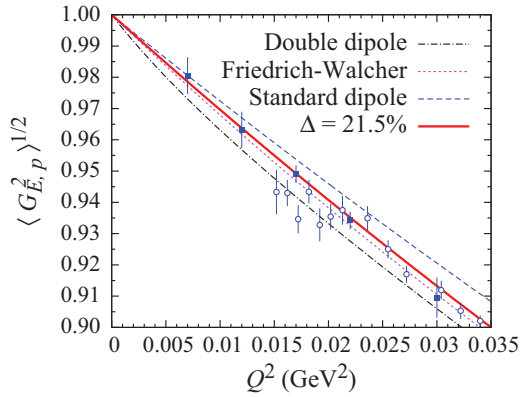

FIG. 5. (Color online) Square root of the averaged $G^2_{E,p}$ obtained from different calculations compared with experimental data for very low Q^2. Notation for experimental data is as in Fig. 1. The result obtained in the present work is represented by the solid curve. Parameters for the double-dipole and Friedrich-Walcher form factors are taken from Ref. [31].

As in the large-Q^2 case, in the very low Q^2 region it is also obvious that the standard dipole form factor is substantially larger than our calculation. The result of our calculation is very close to the result obtained from the Friedrich-Walcher model [43]. Because all four models shown in Fig. 5 yield significantly different proton charge radii, it is of course important to refine the experimental measurement at this kinematics. Theoretically, this is possible because Eq. (1) explicitly shows that at the low-Q^2 contribution of $G_{E,p}$ is dominant. Thus, at low Q^2, measurement of $G_{E,p}$ should be more accurate than that of $G_{M,p}$.

However, from the experimental point of view this could be a daunting task. It should be remembered that measurements of electron-proton scattering cross section for $Q^2 \approx 0.05$ GeV^2 were already at forward angles [31]. Below this point, presumably one has to use other methods. One possible choice proposed at MAMI is the use of the initial-state radiation, i.e., radiation emitted by the electron before it is scattered by the proton, which could provide measurement of form factors down to $Q^2 = 0.0001$ GeV^2 [31]. Obviously, if this method worked, the proton radius would be severely constrained.

IV. EFFECTS OF NUCLEON RADIUS VARIATION ON THE SYMMETRIC NUCLEAR MATTER AND THE NEUTRON STAR MATTER

In the relativistic-mean-field (RMF) model the Lagrangian density of nucleons consists of four terms, i.e., the free nucleon, free meson, interaction between nucleons via meson exchange, and meson self-interaction terms. If we assume that electrons and muons are point particles, whereas nucleons have structures with a radius r_N, then according to the RMF model the energy density of matter consisting of the nucleons and the leptons is given by [39,41]

$$\epsilon = A\left(\epsilon_p^k + \epsilon_n^k\right) + \epsilon_e^k + \epsilon_\mu^k + \epsilon_M(\omega, \sigma, \rho) + g_\omega \omega_0(\rho_p + \rho_n) + \tfrac{1}{2} g_\rho b_0(\rho_p - \rho_n), \quad (9)$$

where g_ω, g_σ, and g_ρ are the couplings for ω, σ, and ρ mesons, respectively, ϵ_M is the total energy density of the meson, while σ, ω_0, and b_0 are the σ, ω, and ρ fields, respectively. Furthermore, in Eq. (9) we have

$$\epsilon_i^k = \frac{2}{(2\pi)^3} \int d^3\vec{k} \left(k^2 + m_i^{*2}\right)^{1/2} \theta(k - k_F), \quad i = p, n, e, \mu, \quad (10)$$

where for leptons the effective mass is $m_i^* = m_i$ and for nucleons it is $m_i^* = m_i - g_\sigma \sigma$.

The nucleon and scalar densities read

$$\rho_i = A\bar{\rho}_i, \quad (11)$$

$$\rho_{s,i} = A\bar{\rho}_{s,i}, \quad (12)$$

where $\bar{\rho}_i$ and $\bar{\rho}_{s,i}$ are the ith nucleon and scalar densities, assuming the nucleon is a point particle. The normalization constant A is given by

$$A = \frac{1}{1 + V_p \bar{\rho}_p + V_n \bar{\rho}_n}, \quad (13)$$

with V_p and V_n the proton and neutron volumes, respectively. To simplify the present calculation we assume that

$$V_p = V_n \equiv V_N = \tfrac{4}{3}\pi r_N^3, \quad (14)$$

where V_N and r_N are the volume and radius of the nucleon, respectively.

From Eq. (9) we can derive the matter pressure,

$$P = \rho^2 \frac{d\varepsilon}{d\rho}, \quad (15)$$

with $\varepsilon = \epsilon/\rho$. Furthermore, the chemical potential for the ith nucleon can be obtained from

$$\mu_i = E_{Fi}^* + V_i P_i' + g_\omega \omega_0 + \alpha_i \tfrac{1}{2} g_\rho b_0, \quad (16)$$

where α_i equals $+1$ (-1) for the proton (neutron), $E_{F,i}^* = (k_{F,i}^2 + m_i^{*2})^{1/2}$, and

$$P_i' = \frac{1}{12\pi^2}\left\{E_{F,i}^* k_{F,i}\left(E_{F,i}^{*2} - \frac{5}{2} m_i^{*2}\right) + \frac{3}{2} m_i^{*4} \log\left(\frac{k_{F,i} + E_{F,i}^*}{m_i^*}\right)\right\}. \quad (17)$$

Differently from the QMC model [34,36], where the dependence of r_N on the matter density can be directly obtained from the model, in the RMF approach the dependence cannot be easily predicted. Therefore, in the present study we choose a phenomenological form for the nucleon radius, which is given by

$$r_N(\rho) = r_N(0)\left\{1 + \beta\left(\frac{\rho}{\rho_0}\right)^2\right\}^{-2}, \quad (18)$$

where $\rho = \rho_p + \rho_n$, ρ_0 is the value of ρ at the saturation point, and $r_N(0)$ is the proton radius in vacuum (zero density), determined from Eq. (7). At first glance, the choice seems to be trivial. However, it is actually selected to fulfill the causality constraint. Furthermore, the formula given in Eq. (18) is more

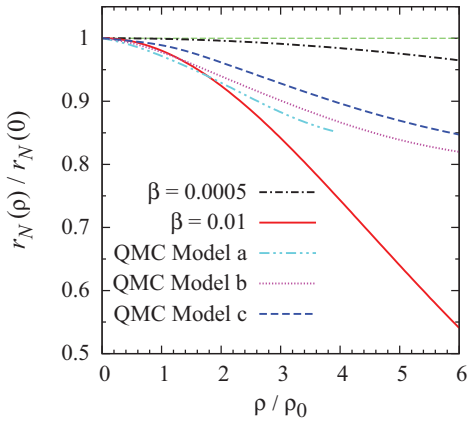

FIG. 6. (Color online) Comparison between proton bag radii as a function of the ratio between nucleon and nuclear saturation densities obtained from the QMC models [34] and Eq. (18) with two β values.

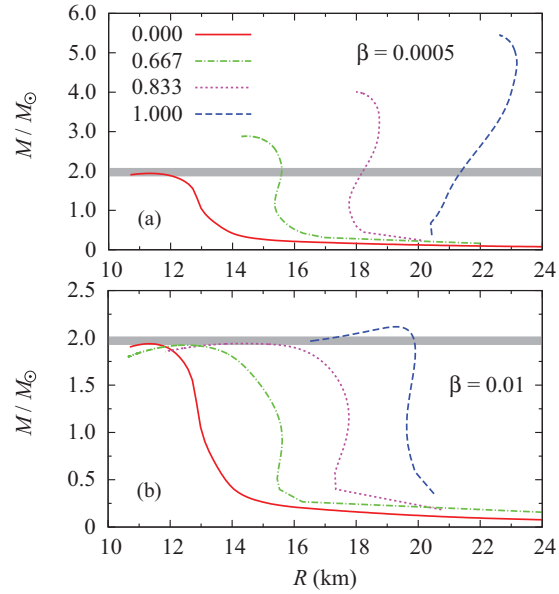

FIG. 7. (Color online) The neutron star mass as a function of its radius for four nucleon radius assumptions. The calculation with (a) $\beta = 0.0005$ and (b) $\beta = 0.01$ in Eq. (18). Gray horizontal bars show the mass of the SRJ164-2230 pulsar, which is believed to be the heaviest observed neutron star [46]. Notation of the curves in both (a) and (b) is given in Fig. 8.

convenient for the present purpose, rather than the exponential one, because in the framework of the presently used RMF model we found that the required radius must slowly fall off as a function of the density. Otherwise, the predicted neutron star mass would violently overshoot the mass of the SRJ164-2230 pulsar, which is believed to be the heaviest observed neutron star [46]. We also observed that, for a selected value of β, Eq. (18) can be adjusted to mimic the result of the QMC models [34] in a certain range of density, thus providing a good check of our result.

The ratio between $r_N(\rho)$ and $r_N(0)$ is exhibited in Fig. 6, where we compare the results obtained from two β values, i.e., $\beta = 0.0005$ and 0.01, with those obtained from the QMC calculation using different values of bag constants B (see Ref. [34] for explanation). It is apparent from this figure that the difference between the calculated radii increases as the density increases. Nevertheless, the distributions of the radii obtained from the QMC model are still bounded within the difference of the two chosen β values in Eq. (18), i.e., the solid and dash-dotted lines in Fig. 6.

For the RMF model we use the parameter set obtained by the IUFSU collaboration [47]. In calculating the EOS of the NSM we use the neutrality and β-stability conditions. They are required in calculating the Fermi momentum of each particle in the neutron star core.

The neutron star mass as a function of its radius can be obtained by solving the Tolman-Oppenheimer-Volkoff equation with different particle densities in the neutron star core. In order to describe the "outer crust" region we have used the EOS given by Rüster *et al.* [48]. The EOS for the "inner crust" region is obtained from an extrapolation of the EOS of the core and outer crust by making use of the polytrophic energy-pressure density approximation. The "crust" region is described by using the RMF model with and without the EVE.

Because in the nuclear matter and NSM a direct comparison between model calculations and precise experimental data, as in the case of electron-proton scattering in the previous section, is beyond our imagination at present, in the following we do not calculate the effect of averaging the nucleon radius on the possible observables. Furthermore, as obtained in the previous section, the effect of this averaging process is a relatively tiny shift from the original value. Therefore, we believe that at this stage it is sufficient to investigate the effect on the conventional observables by using a $\pm 20\%$ variation of the nucleon original radius. Note that this variation enters our calculation through Eqs. (13) and (14).

Figure 7 shows the sensitivity of the neuron star mass-radius relation to the variation of the nucleon radius as well as to the dependence of the nucleon radius on the matter density [β in Eq. (18)], in the framework of RMF models. The radius of the neutron star depends on the value of nucleon radius, whereas the maximum mass of the neutron star is controlled by the dependence of the nucleon radius on the matter density. Therefore, the heaviest observed neutron star mass PSRJ1614-2230 [46], shown by the horizontal gray bars in Fig. 7, yields a significant suppression of the nucleon radius at a very high density. This result is interesting, because it opens the possibility of hyperon existence in a neutron star by using the hyperon vector couplings obtained from SU(6) symmetry [49].

With regard to the radius of the canonical neutron star ($1.4 M_\odot$), which is constrained between 10.4 and 12.9 km [50], our present result should be carefully interpreted, because in this calculation we have used the IUFSU parameter set, which was fitted to the finite nuclei data by assuming point-particle approximation for the nucleon. Therefore, the present result cannot be quantitatively compared with those obtained with other constraints. Nevertheless, Fig. 7 indicates that the present

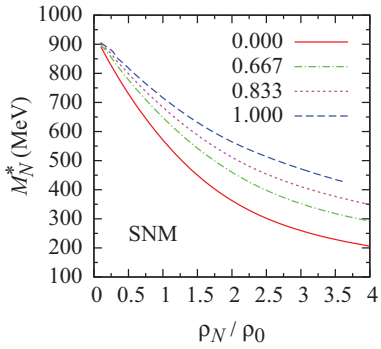

FIG. 8. (Color online) Effective nucleon mass as a function of the ratio between nucleon and nuclear saturation densities. Results were obtained with different values of the nucleon radius $r_N(0)$ as indicated (in fm).

result could become a stringent constraint to the nucleon radius at a high density, once a consistent EOS with EVE is available.

Because the result obtained using $\beta = 0.0005$ substantially overshoots the PSRJ1614-2230 constraint, as shown in Fig. 7, in the following discussion we only use $\beta = 0.01$. The result for the effective nucleon mass in the case of SNM is shown in Fig. 8, where we compare the calculated masses obtained by assuming point particle approximation [$r_N(0) = 0$] and finite nucleon radii [$r_N(0) \neq 0$].

From Fig. 8 it is apparent that at high densities the nucleon effective mass increases with increasing nucleon radius. In view of the instability against the particle-hole excitation at high densities owing to the density fluctuation [51], a sufficiently large effective mass predicted by the RMF model has an obvious advantage.

Figures 9 and 10 exhibit the nonzero nucleon radius effect on the EOS of SNM and NSM, respectively. The filled circles in the NSM EOS in Fig. 10 indicate the positions of the nuclear star center pressures and center energy densities of maximum mass. At moderate densities, which correspond to $\epsilon \lesssim 300$, we observe that the EOS becomes stiffer as the nucleon radius increases. Beyond this range, the EOS tends to be softer. From Fig. 11, it is obvious that the pressure of the nuclear star center with maximum mass of $r_N(0) = 1$ fm [dashed (blue) line] is approximately 32 MeV fm^{-3}, which corresponds to the energy density of about 320 MeV fm^{-3}. At this point the EOS obtained with $r_N(0) = 1$ fm is stiffest compared to the other cases [Fig. 10(a)]. Because in obtaining the nuclear star mass we should integrate the Tolman-Oppenheimer-Volkof equation using the corresponding EOS as input from the nuclear star center pressure up to 0, information based solely on the soft EOS at high densities of $r_N(0) = 1$ fm is insufficient for a complete understanding of the neutron star maximum mass. For other nonzero nucleon radius cases, the situation is similar.

Obviously, decreasing the nucleon radius will decrease the pressure in the region of $\epsilon \leqslant 300$ MeV fm^{-3}. However,

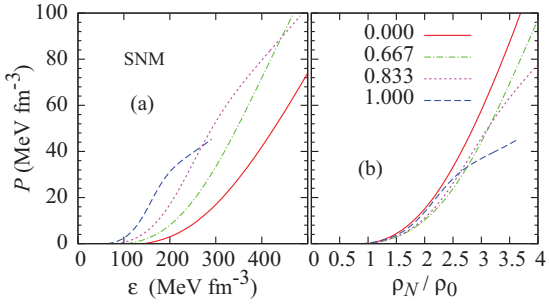

FIG. 9. (Color online) Equation of states of the symmetric nuclear matter obtained from calculations with different values of the nucleon radius as a function of (a) energy and (b) density. Notation of the curves is as in Fig. 8.

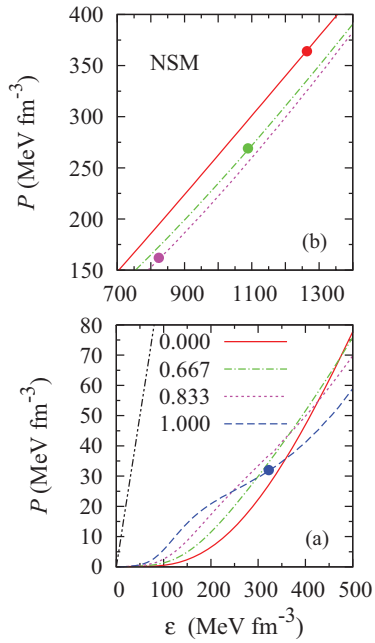

FIG. 10. (Color online) As Fig. 9(a), but for neutron star matter at (a) lower and (b) higher energies. (a) The dash-dot-dotted line in shows the causality constraint, and the filled circles indicate the center pressures and energy densities in the neutron star with maximum mass.

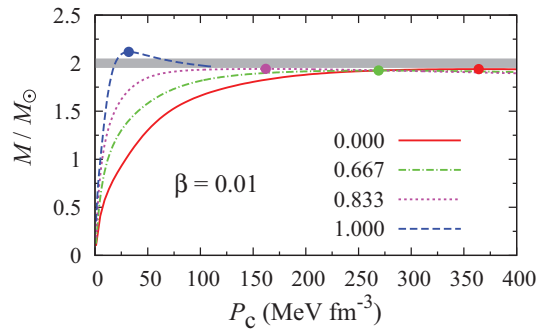

FIG. 11. (Color online) Neutron star mass as a function of its center pressure for different nucleon radii obtained with $\beta = 0.01$. Filled circles indicate the maximum masses with the corresponding center pressures.

decreasing the nucleon radius will simultaneously increase the nuclear star center pressure. Thus, an additional contribution from the center pressure up to 300 MeV fm^{-3} will only slightly increase the nuclear star mass. This is because the corresponding EOSs at high densities are relatively soft. On the other hand, in the case of zero nucleon radius but using the same RMF parameter set, the contribution from 300 MeV fm^{-3} up to 0 is very small but the contribution from high densities is dominant because the corresponding EOS is stiffer than that of the nonzero nucleon radius. The very small contribution in the region $\leqslant$300 MeV fm^{-3} and the relatively large center pressure are typical for point-particle RMF models. In this case, the strong correlation between the nuclear star maximum mass and the EOS stiffness at high densities is very obvious. Therefore, in the point-particle case we only need to consider the EOS at high densities in investigating the nuclear star maximum mass behavior. In addition, the high-density EOSs become significantly stiffer as β decreases, As a consequence, decreasing the β value will increase the maximum neutron star mass. Thus, the increase in the nuclear star mass depends sensitively on the nucleon radius in free space. These phenomena explain the increase in the predicted mass and radius of the neutron star with increasing nucleon radius, as shown in Fig. 7.

In Fig. 12 we display the finite nucleon radius effect on the fraction of the matter constituents in the neutron star. It is obvious from this figure that increasing the nucleon radius will increase the number of existing charge particles at a high density. This result has serious consequences for a number of neutron star properties, such as neutron star stability, neutrino transport in the neutron star, and the cooling process of a neutron star. Unfortunately, a more detailed and quantitative analysis of the EVE on a neutron star should wait for a more consistent EOS, which includes the EVE in the calculation.

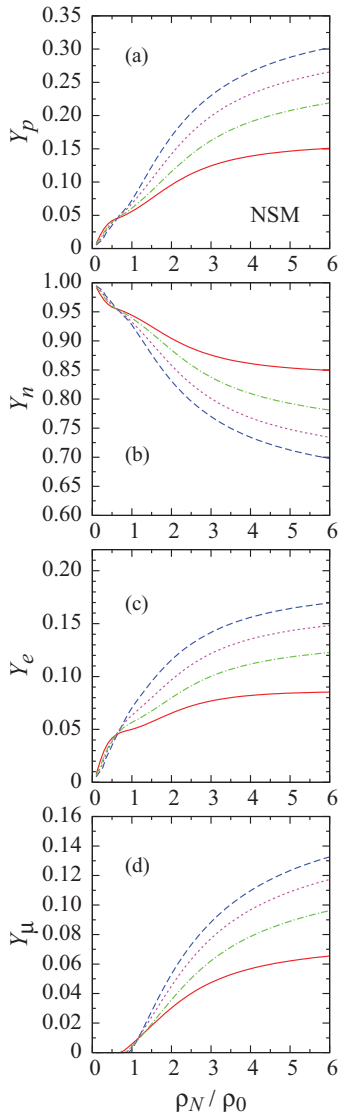

FIG. 12. (Color online) Proton, neutron, electron, and muon fractions in the neutron star matter as a function of the ratio between nucleon and nuclear saturation densities. Notation of the curves is as in Fig. 8.

V. SUMMARY AND CONCLUSION

We have investigated effects of proton radius variation on extraction of the proton charge form factor. To achieve the best agreement with experimental data we have averaged a dipole form factor over the corresponding cutoff, with an upper (lower) integration limit of +21.5% (−21.5%) from its middle value. The extracted proton charge radius is found to be smaller than that obtained using the traditional standard dipole fit but is in good agreement with those obtained from a recent measurement of the Lamb shift in a muonic hydrogen atom as well as from the dispersion relation. The extracted proton magnetic radius is smaller than the result of the dispersion relation but in agreement with the direct extraction making use of the Friedrich-Walcher form factor. Nevertheless, as the magnetic form factor is less accurate, the extraction of the magnetic radius is also less reliable compared to the result for the charge radius.

We have also investigated effects of nucleon radius variation on the SNM and the NSM. To this end, the nucleon radius dependence on the matter density is described by a simple phenomenological form and four assumptions of the nucleon radius at zero density are considered in the calculation, i.e., 0 fm (point-particle approximation), 0.833 fm (original radius), as well as 0.667 fm and 1.000 fm (±20% modifications of the original radius). We found that the relation between the mass and the radius of a neutron star is very sensitive to the radius of the nucleon. A similar result is also observed in the case of the effective nucleon mass of the SNM as well as the EOS of both NSM and SNM. However, a more quantitative conclusion can be drawn only after a more consistent EOS, with the EVE considered, is available.

ACKNOWLEDGMENTS

This work was supported in part by the University of Indonesia and the Competence Grant from the Indonesian Ministry of Education and Culture.

[1] R. Pohl *et al*., Nature **466**, 213 (2010).
[2] P. J. Mohr, B. N. Taylor, and D. B. Newell, Rev. Mod. Phys. **80**, 633 (2008).
[3] J. C. Bernauer *et al*. (A1 Collaboration), Phys. Rev. Lett. **105**, 242001 (2010).
[4] G. A. Miller, A. W. Thomas, J. D. Carroll, and J. Rafelski, Phys. Rev. A **84**, 020101 (2011).
[5] G. A. Miller, A. W. Thomas, and J. D. Carroll, Phys. Rev. C **86**, 065201 (2012).
[6] J. Jaeckel and S. Roy, Phys. Rev. D **82**, 125020 (2010).
[7] A. De Rujula, Phys. Lett. B **693**, 555 (2010).
[8] I. C. Cloet and G. A. Miller, Phys. Rev. C **83**, 012201 (2011).
[9] D. Tucker-Smith and I. Yavin, Phys. Rev. D **83**, 101702 (2011).
[10] B. Batell, D. McKeen, and M. Pospelov, Phys. Rev. Lett. **107**, 011803 (2011).
[11] R. J. Hill and G. Paz, Phys. Rev. Lett. **107**, 160402 (2011).
[12] V. Barger, C.-W. Chiang, W.-Y. Keung, and D. Marfatia, Phys. Rev. Lett. **106**, 153001 (2011).
[13] J. D. Carroll, A. W. Thomas, J. Rafelski, and G. A. Miller, Phys. Rev. A **84**, 012506 (2011).
[14] U. D. Jentschura, Ann. Phys. **326**, 500 (2011); **326**, 516 (2011).
[15] P. Brax and C. Burrage, Phys. Rev. D **83**, 035020 (2011).
[16] J. I. Rivas, A. Camacho, and E. Göklü, Phys. Rev. D **84**, 055024 (2011).
[17] A. Pineda, Presentation at 14th International Conference on Hadron Spectroscopy (Hadron 2011), arXiv:1108.1263 [hep-ph].
[18] C. E. Carlson, V. Nazaryan, and K. Griffioen, Phys. Rev. A **83**, 042509 (2011).
[19] V. Barger, C.-W. Chiang, W.-Y. Keung, and D. Marfatia, Phys. Rev. Lett. **108**, 081802 (2012).
[20] E. Borie, Ann. Phys. **327**, 733 (2012).
[21] M. I. Eides, Phys. Rev. A **85**, 034503 (2012).
[22] M. C. Birse and J. A. McGovern, Eur. Phys. J. A **48**, 120 (2012).
[23] M. O. Distler, J. C. Bernauer, and T. Walcher, Phys. Lett. B **696**, 343 (2011).
[24] I. T. Lorenz, H.-W. Hammer, and U.-G. Meissner, Eur. Phys. J. A **48**, 151 (2012).
[25] N. G. Kelkar, F. G. Daza, and M. Nowakowski, Nucl. Phys. B **864**, 382 (2012).
[26] A. Kvinikhidze and G. A. Miller, Phys. Rev. C **73**, 065203 (2006); **76**, 025203 (2007).
[27] F. Gross and P. Agbakpe, Phys. Rev. C **73**, 015203 (2006).
[28] V. Yu. Denisov, Eur. Phys. J. A **47**, 80 (2011).
[29] J. P. Ralston and B. Pire, Phys. Rev. Lett. **61**, 1823 (1988).
[30] A. S. Carroll *et al*., Phys. Rev. Lett. **61**, 1698 (1988).
[31] J. C. Bernauer, Ph.D. thesis, Universität Mainz (2010).
[32] A. Antognini *et al*., Science **339**, 417 (2013).
[33] B.-X. Sun, X.-F. Lu, and E.-G. Zhao, Phys. Rev. C **65**, 054301 (2002).
[34] R. M. Aguirre and A. L. De Paoli, Phys. Rev. C **68**, 055804 (2003).
[35] R. M. Aguirre and A. L. De Paoli, Phys. Rev. C **75**, 045207 (2007).
[36] P. K. Panda, M. E. Bracco, M. Chiapparini, E. Conte, and G. Krein, Phys. Rev. C **65**, 065206 (2002).
[37] B. K. Patra and C. P. Singh, Nucl. Phys. A **614**, 337 (1997).
[38] D. V. Anghel, A. S. Parvan, and A. S. Khvorostukhin, Physica A **391**, 2313 (2012).
[39] H. Kouno, K. Koide, T. Mitsumori, N. Noda, and A. Hasegawa, Prog. Theor. Phys. **96**, 191 (1996).
[40] F. Halzen and A. D. Martin, in *Quarks and Leptons: An Introductory Course in Modern Particle Physics* (John Wiley & Sons, New York, 1984), p. 175.
[41] D. H. Rischke, M. I. Gorenstein, H. Stöker, and W. Greiner, Z. Phys. C **51**, 485 (1991).
[42] J. Arrington, W. Melnitchouk, and J. A. Tjon, Phys. Rev. C **76**, 035205 (2007).
[43] J. Friedrich and Th. Walcher, Eur. Phys. J. A **17**, 607 (2003).
[44] J. Arrington, Phys. Rev. C **69**, 022201 (2004).
[45] E. L. Lomon, Phys. Rev. C **64**, 035204 (2001).
[46] P. B. Demorest, T. Pennuci, S. M. Ransom, M. S. E. Roberts, and J. W. T. Hessels, Nature **467**, 1081 (2010).
[47] F. J. Fattoyev, C. J. Horowitz, J. Piekarewicz, and G. Shen, Phys. Rev. C **82**, 055803 (2010).
[48] S. B. Rüster, M. Hempel, and J. Schaffner-Bielich, Phys. Rev. C **73**, 035804 (2006).
[49] S. Weissenborn, D. Chatterjee, and J. Schaffner-Bielich, Phys. Rev. C **85**, 065802 (2012).
[50] A. W. Steiner, J. M. Lattimer, and E. F. Brown, Astrophys. J. Lett. **765**, L5 (2013).
[51] A. Sulaksono, T. J. Bürvenich, P.-G. Reinhard, and J. A. Maruhn, Phys. Rev. C **79**, 044306 (2009).